



**HAL**  
open science

# Recovering effective thicknesses and optical properties of copper and copper oxide layers from absorbance measurements

Dominique Barchiesi, Deniz Cakir, Thomas Grosjes, Nicole Fréty, Eric Anglaret

## ► To cite this version:

Dominique Barchiesi, Deniz Cakir, Thomas Grosjes, Nicole Fréty, Eric Anglaret. Recovering effective thicknesses and optical properties of copper and copper oxide layers from absorbance measurements. *Optical Materials*, 2019, *Optical Materials*, 91, pp.138-146. 10.1016/j.optmat.2019.02.029 . hal-02077581

**HAL Id: hal-02077581**

**<https://inria.hal.science/hal-02077581>**

Submitted on 22 Oct 2021

**HAL** is a multi-disciplinary open access archive for the deposit and dissemination of scientific research documents, whether they are published or not. The documents may come from teaching and research institutions in France or abroad, or from public or private research centers.

L'archive ouverte pluridisciplinaire **HAL**, est destinée au dépôt et à la diffusion de documents scientifiques de niveau recherche, publiés ou non, émanant des établissements d'enseignement et de recherche français ou étrangers, des laboratoires publics ou privés.



Distributed under a Creative Commons Attribution - NonCommercial 4.0 International License

# Recovering effective thicknesses and optical properties of copper and copper oxide layers from absorbance measurements

Dominique Barchiesi<sup>a,\*</sup>, Deniz Cakir<sup>b</sup>, Thomas Grosge<sup>a</sup>, Nicole Fréty<sup>c</sup>, Eric Anglaret<sup>b</sup>

<sup>a</sup>Group for Automatic Mesh Generation and Advanced Methods (GAMMA3) - Université de technologie de Troyes - INRIA - CS 42060 - 10004 Troyes Cedex - France

<sup>b</sup>Laboratoire Charles Coulomb - UMR CNRS 5221 - Université de Montpellier - CC069 - Place Eugène Bataillon - F-34095 Montpellier Cedex 5 - France

<sup>c</sup>Institut Charles Gerhardt - UMR CNRS 5253 - Université de Montpellier - CC1504 - Place Eugène Bataillon - F-34095 Montpellier Cedex 5 - France

---

## Abstract

Nowadays, the recovering of both thicknesses and optical properties of nanometric multilayers is still a challenge. We propose a method to recover the effective relative permittivities and the thicknesses of copper/copper oxide layers, from absorbance **spectra measured** in the visible spectra. The experimental data are fitted with a model of classical light-matter interaction and a combination of two Drude-Lorentz laws to calculate the relative permittivities over the spectrum. The Particle Swarm Optimization and the evolutionary methods are used for the least-square fitting. A two steps study reveals that the relative permittivities of bulk cannot be used to fit adequately the absorbance curves. However, a perturbation of these reference values improves their fitting. The method is applied to the absorption spectra of a set of three **copper** samples that are progressively oxidized by six successive heat treatments.

**Keywords:** Optical properties of multilayers, optical properties of films, Inverse problems, Optical transmission coefficients

**PACS:** 78.67.Pt, 78.20.-e, 78.66.-w, 02.30.Zz, 78.20.Ci

---

## 1. Introduction

Recovering the thickness and the optical properties of deposited nanolayers is a current challenge in nanotechnologies [1]. Knowing those physical quantities could help the physic of layer

---

\*Corresponding author

Email address: [dominique.barchiesi@utt.fr](mailto:dominique.barchiesi@utt.fr) (Dominique Barchiesi)

4 deposition and the related engineering. Indeed, multilayers are used in the fabrication of many  
5 optical devices [1] and sensors [2] (e.g. based on SPR: Surface Plasmon Resonance [3, 4] and/or  
6 SERS: Surface Enhanced Resonance Spectroscopy [5, 6]). These devices are used for molecular  
7 detection, and optimized to get the highest sensitivity [7]. The joint measurement of thicknesses  
8 and optical properties is an issue. With ellipsometry, the knowledge of the optical properties of ma-  
9 terials is required to determine its thickness. Moreover, the roughness of nanolayers [8, 9, 10, 11]  
10 and their structures [12] depend on the deposition method. The oxidation of metal nanolayers  
11 cannot be neglected. The structure of copper and native copper oxide depends on the fabrica-  
12 tion method [13, 14, 15, 16, 17]. The post-annealing of copper nanolayers induces copper oxida-  
13 tion [18, 19, 20, 21], structural-changes and variations of the optical properties [22, 23]. Oxidation  
14 is a complex phenomenon, which is temperature dependent [24, 25, 26] and the oxidation kinetics  
15 can be found in Ref. [17]. Consequently, optical properties can significantly vary from sample to  
16 sample and should be jointly determined with the thicknesses.

17 To address this problem, we propose here to evaluate the effective thicknesses and the effec-  
18 tive optical properties of thin layers of copper from the fit of experimental curves of absorbance.  
19 The model used for fitting is a Fresnel model of transmittance for the absorbance [27] and two  
20 combinations of two Drude-Lorentz laws to describe the dispersion of either copper or copper ox-  
21 ide [28]. The Particle Swarm optimization and the Evolutionary methods are also used for fitting  
22 the experimental data.

23 The results could be used for further applications (SPR, spectroscopy, SERS. . . ) and for com-  
24 parison between the samples recovered, obtained from various fabrication techniques. The paper  
25 is organized as follow. Section 2 is devoted to the sample preparation, the methods of characteri-  
26 zation and to the presentation of the numerical methods. Section 3 shows the experimental data of  
27 absorbance and the fit results, first assuming the bulk optical properties, and second considering  
28 the relative permittivities of copper and of copper oxide as degrees of freedom, in addition to the  
29 thicknesses. These results are discussed before concluding.

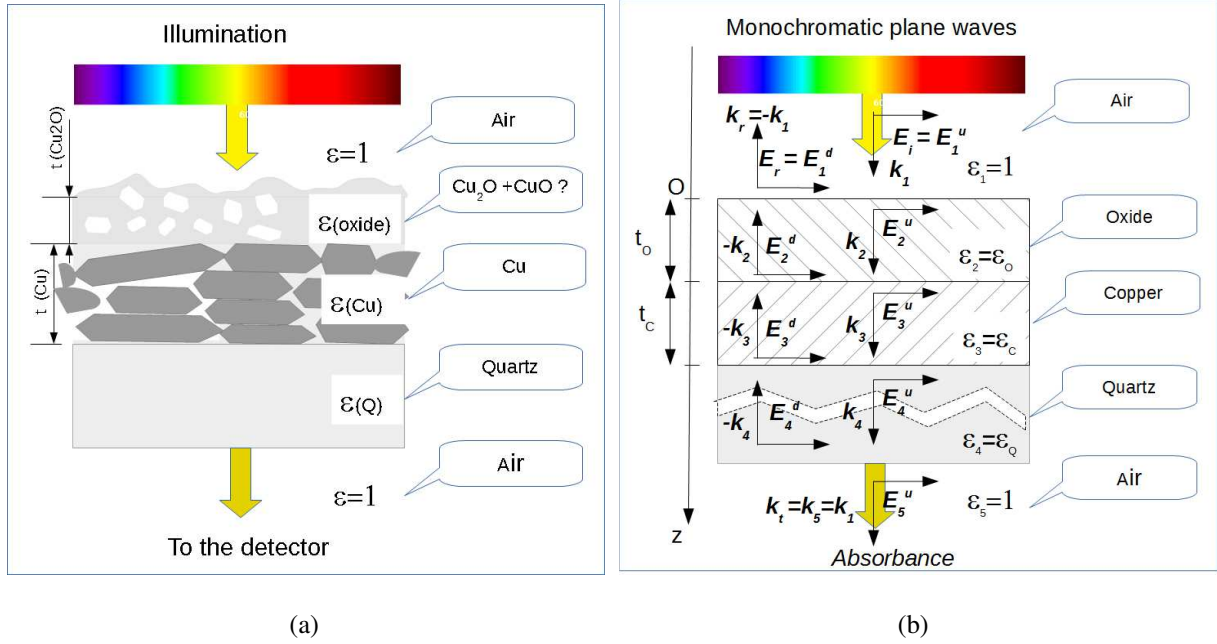


Figure 1: (a) Presumed structure of copper/copper oxide bilayer. (b) schematic of the electromagnetic model of interaction of light with the copper/copper oxide bilayer.

## 2. Materials and Methods

### 2.1. Sample preparation and first characterization

The copper nanolayers are deposited by thermal evaporation on fused silica substrates (optical grade from Neyco). Prior to deposition, the substrates are cleaned in an acetone bath with ultrasounds for 5 minutes, and then plasma-treated in a 70%  $O_2$  / 30%  $N_2$  atmosphere for 6 minutes. The copper wire of purity of 99,999%, bought from Alfa Aesar is placed 18 cm below the target substrate. The sublimation of the  $Cu$  wire is achieved under 120 A, at  $10^{-5}$  mbar, using a tungsten crucible as the counter-electrode. The target thicknesses (nominal thickness before oxidation) of copper layers are  $t_C^n = 10$  nm, 30 nm and 50 nm. Figure 1 shows a schematic of the bilayer on quartz substrate.

The actual thicknesses are determined by Atomic Force Microscopy (AXS Bruker used in tapping mode using silicon nitride cantilevers with sharpened pyramidal tips, with a residual noise of  $\pm 0.5 \text{ \AA}$ ), from the measurement of the average height of the substrate/layer steps, and by ellipsometry (using a Nanofilm EP4 spectroscopic ellipsometer working at a fixed incident angle of  $50^\circ$

Target thickness $t_C^n$	AFM		ellipsometry	
	$t_C + t_O$ (nm)	$t_C$ (nm)	$t_O$ (nm)	$t_C + t_O$ (nm)
10 nm	$11.0 \pm 3.0$	$11.0 \pm 0.2$	$3.4 \pm 0.2$	$14.4 \pm 0.3$
30 nm	$31.0 \pm 5.0$	$38.7 \pm 1.3$	$3.7 \pm 0.2$	$42.4 \pm 1.3$
50 nm	$51.0 \pm 8.0$	--	$5 \pm 0.9$	--

Table 1: AFM and ellipsometry characterization of the thicknesses of copper and copper oxide. The uncertainties for AFM correspond to standard deviations of the thickness of the layers, while they are the standard deviation of the fit parameters of the experimental data for ellipsometry. The uncertainty of  $t_C + t_O$  is calculated from uncertainties on  $t_C$  and  $t_O$  by using the square root of the sum of square [29].

with several monochromatic incident radiations at 560, 660, 760, 860 and 960 nm), assuming a bilayer of copper/copper oxide and the permittivities of bulk copper and copper oxide [30]. The AFM and ellipsometry results are compared in Tab. 1, where  $t_C$  and  $t_O$  refer to the thicknesses of copper and of copper oxide, respectively. The copper thickness of the 50 nm sample is too large to be determined by ellipsometry because of its too high absorbance. Table 1 also gives the experimental uncertainties on the measurements of thicknesses for both AFM and ellipsometry. Such uncertainties are related to the roughness of the samples for AFM and to the fits of the data for ellipsometry (about 15-27% for AFM and about 3-8% for ellipsometry). Discrepancies between AFM and ellipsometry measurements of the thickness  $t_C + t_O$  can be observed. This suggests that the use of the permittivities of bulk copper and copper oxide is not relevant for thin layers, as will be demonstrated further in this work.

Copper thin films were annealed under air at atmospheric pressure. The annealing temperatures were chosen to be low enough to preferentially form  $\text{Cu}_2\text{O}$ . Based on literature [16, 18, 21, 31, 32], thin films were annealed in the range of 120-170°C. The samples were introduced in the furnace previously heated at the annealing temperature and straightly removed after annealing for cooling at room temperature. Annealing was performed progressively, for increasing times  $T$  and temperatures  $\theta$  following the thermal treatment as detailed in Tab. 2. The evolution of the oxidation was studied by UV-vis absorbance measurements for each annealing condition on a Cary 5000 spectrometer over the spectral range 400-800 nm, using a beam diameter of 1 mm.

Time $T$ (min)	Temperature $\theta$ ( $^{\circ}C$ )
0	0
102	120
190	120
240	130
600	130
900	170

Table 2: Annealing times and temperatures for the thermal treatments (annealing) of each sample of target thickness 10, 30, 50 nm.

Therefore, 18 absorption spectra are available for fitting by the model described in the following subsection.

## 2.2. The model of absorbance

The absorbance  $A_{exp}(\lambda_0)$  is deduced from the transmittance of the sample, that is illuminated in normal incidence by a linearly polarized plane wave, neglecting the scattering. Therefore, the recovered thicknesses and optical properties are effective values. Figure 1 shows a sketch of the possible material structure of a copper-copper oxide bilayer and a schematic of the plane multilayer model. The bilayer model for the light-material interaction is based on the Fresnel coefficients in normal incidence. The numerical calculation was described in Ref [33]. The calculation of the absorbance is then deduced from the transmission coefficient  $t_{14}$ :

$$A(\omega, t_C, t_O, \epsilon_G, \epsilon_C, \epsilon_O, \epsilon_A) = -\log \left[ |t_{14}|^2 \left| \frac{2n_Q}{n_Q + n_A} \right|^2 \right], \quad (1)$$

where  $n_Q = \epsilon_Q^{1/2}$  is the refractive index of the quartz substrate [34] and  $n_A = 1$  is the optical index of air. Both the measured data and the calculations are limited to the visible spectrum: the incident wavelength of illumination  $\lambda_0$  belongs to [400; 800] nm. The relative permittivities  $\epsilon_G$ ,  $\epsilon_C$ , and  $\epsilon_O$  are function of  $\lambda_0$ . Optimization methods are used to fit the experimental absorbance curves by the numerical model.

78 2.3. The methods for fitting

The goal is to find the best inputs of the model that minimize the difference between the measured data and the calculations. This problem belongs either to the curves fitting strategies or to the inverse problem resolution. Here, the fitting function comes from a physical model and therefore the goal is to solve the inverse problem. The recovered parameters of the model are obtained from the minimum of the fitness function or objective function in optimization methods. The fitness function is defined as the square root of the sum of the squared residuals (for each angular frequency), divided by the number of measured values over the spectra ( $N_\omega = 401$ ) :

$$E_f = \sqrt{\frac{\sum_{i=1}^{N_\omega} |\text{Measured}(\omega_i) - \text{Calculated}(\omega_i)|^2}{N_\omega}}. \quad (2)$$

The Drude-Lorentz laws are defined as functions of the angular frequency, therefore both relative permittivity and absorbance curves are fitted as functions of the angular frequency  $\omega \in [2.35; 4.71] \times 10^{15}$  rad/s. The relative error of fit (in %) is also of interest to visualize the quality of fit over the spectrum:

$$RE_f(\lambda_i) = 100 \left| 1 - \frac{\text{Calculated}(\lambda_i)}{\text{Measured}(\lambda_i)} \right|, \quad (3)$$

79 where  $\lambda_i = 2\pi c/\omega_i$ , with  $c$  the speed of light in vacuum.

80 Among the numerous methods proposed to solve the inverse problem, the metaheuristic meth-  
 81 ods of optimization are of interest [29]. The basic Particle Swarm Optimization (PSO) is probably  
 82 one of the most simple to implement numerically. The PSO was successfully used to fit the re-  
 83 fractive index of metals [28] and to recover unknown geometrical and material parameters of  
 84 aluminum nanolayers and nanoparticles [35, 36]. Genetic algorithm (GA) has also been used to fit  
 85 experimental data [37, 38, 39]. All the inputs of the model (particle) are first randomly generated  
 86 in the domain of search before beginning the evolutionary loop.

- 87 • PSO : the input parameters are moved to another region of the domain of search along a  
 88 vector of translation which is a function of the best position of the particle, the best position  
 89 of the swarm and the previous translation vectors [40].

- GA : the input parameters are varied by using recombination, mutation and selection operators.

The fitness function  $E_f$  (Eq. 2) is evaluated for each new set of parameters. The best set of input parameters of the model is obtained for the minimum of the fitness function. The evolutionary loop ends if the stop criterion is reached ( $E_f \leq 0.01$ ) or if the number of iterations of the evolutionary loop is equal to the maximum allowed (typically  $10^4$  or  $2 \times 10^4$ ). Hundred realizations of the same algorithm help to test the stability of the method.

Both method give the same results in comparable calculation times and memory requirements, for a wide range of tuning parameters of each method of optimization. These methods are used to fit the bulk relative permittivities with combination of two Drude-Lorentz laws, and to solve the inverse problem of absorbance.

#### 2.4. Fitting the relative permittivities of bulk copper and bulk copper oxide

First, the optical properties of copper and copper oxide [30] are fitted by a combination of two Drude-Lorentz laws of dispersion [28]. The choice of these reference data was based on a pre-study using several data sets for the optical properties. We used a Monte-Carlo method [29] to evaluate the influence of the propagation of uncertainties on experimental fits. The reference data is the one that gave the best results. A combination of Drude and Drude-Lorentz laws was also tested and gave worse results. Therefore, a single function (the combination of two Drude-Lorentz laws) is able to describe the relative permittivities on the whole domain of investigated wavelengths in the experimental data. The relative permittivity of each medium  $\epsilon(\omega) = (n + i\kappa)^2$  is the square of the complex refractive index, which depends on the angular frequency  $\omega$ . The fitting function is:

$$\epsilon(\omega) = \epsilon_\infty - \frac{\Delta\omega_1^2}{\omega^2 - \omega_1^2 + i\Gamma_1\omega} - \frac{\Delta\omega_2^2}{\omega^2 - \omega_2^2 + i\Gamma_2\omega}. \quad (4)$$

The least square distance between the measured reference and the fit is minimized by using the same method as described in Ref [28]. The results are plotted in Figs 2-3. Table 3 gives the recovered parameters (Eq. 4) of the fit of the relative permittivity of copper and copper oxide. We use this first set of parameters as a starting point to fit the absorbance over the visible spectra.

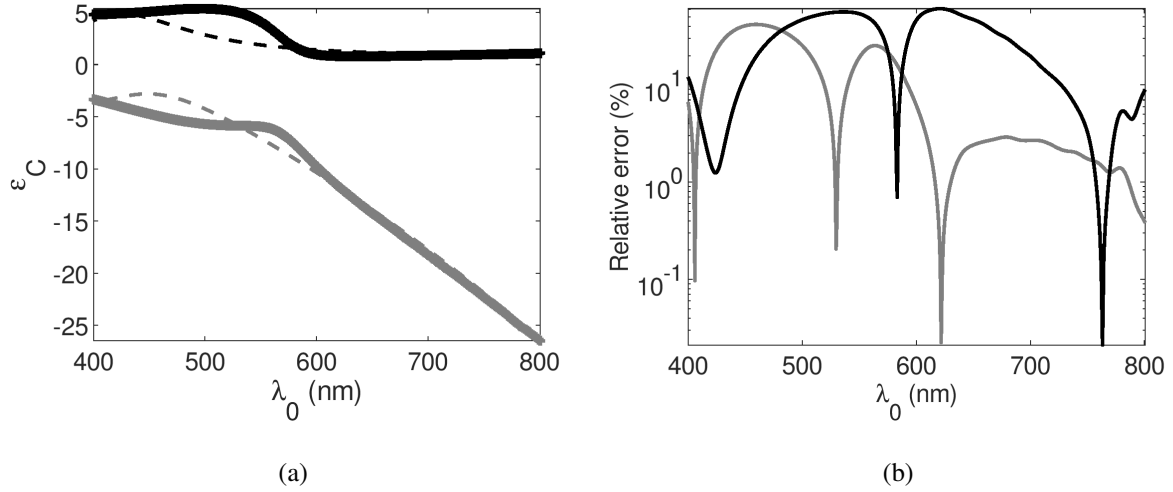


Figure 2: (a) Solid lines: real (gray) and imaginary (black) parts of the relative permittivity of copper from [19]. The dashed lines show the result of the fit with two Drude-Lorentz laws. (b) Relative error of fit (Eq. 3).

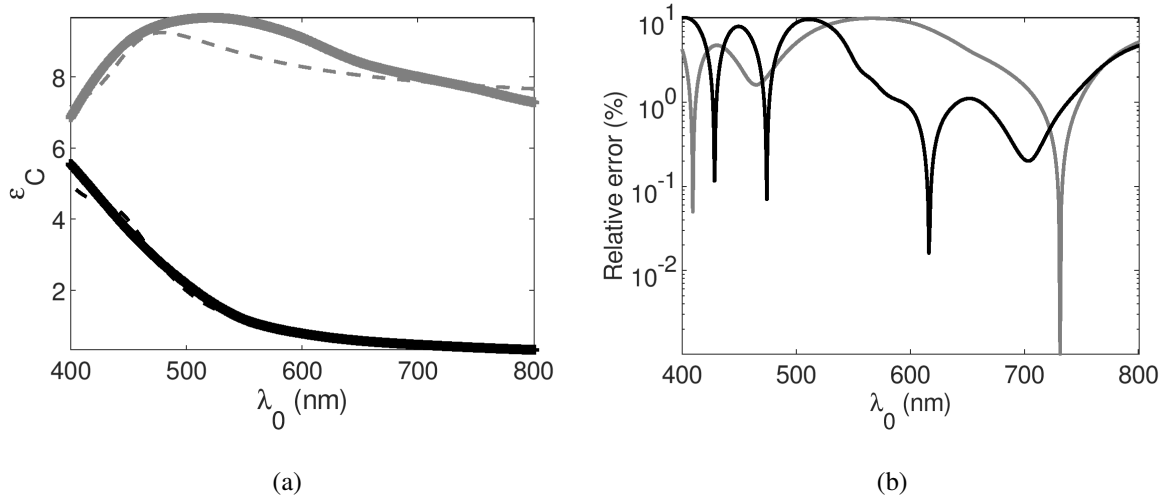


Figure 3: (a) Solid lines: real (gray) and imaginary (black) parts of the relative permittivity of copper oxide from [30]. The dashed lines show the result of the fit with two Drude-Lorentz laws. (b) Relative error of fit (Eq. 3).

	Copper	Copper oxide
$\epsilon_\infty$	5.8511	5.3496
$\Gamma_1$	$3.0361 \times 10^{13}$	$8.8356 \times 10^{14}$
$\omega_1$	$5.5572 \times 10^{14}$	$4.2802 \times 10^{15}$
$\Delta\omega_1$	$1.3395 \times 10^{16}$	$2.9672 \times 10^{15}$
$\Gamma_2$	$1.5255 \times 10^{15}$	$1.2495 \times 10^{15}$
$\omega_2$	$4.4831 \times 10^{15}$	$5.1533 \times 10^{15}$
$\Delta\omega_2$	$5.6938 \times 10^{15}$	$5.9297 \times 10^{15}$

Table 3: Best parameters of Eq. 4 recovered from reference data of the relative permittivity of copper and copper oxide [19].

### 116 3. Results and discussion

117 A first step consists in recovering the effective thicknesses of the copper and copper oxide  
118 layers, assuming that the optical properties of the thin layers are those of the bulk materials. In  
119 this case, two unknowns must be recovered: the effective thickness of copper and that of copper  
120 oxide. The second step consists in relaxing the effective thicknesses values, as well as the optical  
121 properties of the materials, in order to improve the fits of absorbance. In this case, the two effective  
122 thicknesses and the 14 parameters must be recovered (7 for each of the 2-Drude-Lorentz laws, one  
123 for each material).

#### 124 3.1. First step: recovering of effective thicknesses assuming optical properties of bulk materials

125 First, we deduce the two effective thicknesses from the best fit of the absorbance curves, as-  
126 suming the optical properties of bulk materials (Tab. 3 and Eq. 4). The recovered effective thick-  
127 nesses of copper and copper oxide are shown in Tab. 4 (superscript <sup>a</sup>). For each group of samples  
128 (target thicknesses 10, 30, 50 nm), the effective thickness of copper decreases (and that of oxide  
129 increases) with increasing oxidation time  $T$ . Nevertheless, the total effective thickness appears to  
130 be larger than the thickness that is measured with AFM (Tab. 1). **Note that the results are closer**  
131 **to the ellipsometry measurements, especially for the 10 nm sample, which is not surprising since**  
132 **bulk optical properties are used to calculate the thicknesses.**

$t_C^n$ (nm), $T$ (min)	$E_f^a$	$t_C^a$ (nm)	$t_O^a$ (nm)	$E_f^b$	$t_C^b$ (nm)	$t_O^b$ (nm)	$t_C^b + t_O^b$ (nm)
<b>10, 0</b>	<b>0.08</b>	<b>12</b>	<b>6</b>	<b>0.009</b>	<b>11.0 (0.7)</b>	<b>4.3 (0.4)</b>	<b>15.3 (0.8)</b>
10, 102	0.1	9	10	0.009	10.3 (0.5)	4.4 (0.4)	14.7 (0.6)
10, 190	0.1	8	12	0.009	7.7 (0.6)	6.6 (0.6)	14.3 (0.8)
10, 240	0.04	0	20	0.008	6.9 (1.3)	7.7 (2.2)	14.6 (2.6)
10, 600	0.04	3	19	0.004	0.1 (0.0)	13.7 (0.1)	13.8 (0.1)
10, 900	0.04	3	20	0.004	0.1 (0.1)	14.3 (2.2)	14.4 (2.2)
<b>30, 0</b>	<b>0.2</b>	<b>38</b>	<b>6</b>	<b>0.02</b>	<b>32.9 (1.7)</b>	<b>4.9 (0.4)</b>	<b>37.8 (1.7)</b>
30, 102	0.1	34	10	0.02	30.8 (1.6)	9.1 (0.6)	39.9 (1.7)
30, 190	0.1	32	12	0.02	23.4 (0.0)	11.1 (0.0)	34.5 (0.6)
30, 240	0.2	24	26	0.03	15.9 (1.8)	11.2 (1.2)	27.1 (2.2)
30, 600	0.2	21	32	0.05	15.2 (1.5)	14.0 (0.9)	29.2 (1.7)
30, 900	0.07	0	63	0.02	9.4 (1.0)	23.0 (1.4)	32.4 (1.7)
<b>50, 0</b>	<b>0.3</b>	<b>63</b>	<b>18</b>	<b>0.04</b>	<b>53.2 (1.7)</b>	<b>4.5 (1.2)</b>	<b>57.7 (2.1)</b>
50, 102	0.2	58	17	0.04	51.1 (1.5)	13.8 (1.6)	64.9 (2.2)
50, 190	0.2	56	19	0.05	50.5 (1.6)	22.8 (0.9)	73.3 (1.8)
50, 240	0.1	48	27	0.04	33.2 (1.4)	32.1 (2.5)	65.3 (2.9)
50, 600	0.2	43	35	0.1	32.5 (0.7)	40.2 (3.8)	72.7 (3.9)
50, 900	0.08	0	108	0.009	0.9 (0.0)	101.7 (0.0)	102.6 (0.0)

Table 4: Sample (nominal thickness of copper  $t_C^n$ , oxidation time  $T$ ), fitness function  $E_f$ , recovered effective thicknesses of copper  $t_C$  and copper oxide  $t_O$ . The superscripts  $a$  and  $b$  indicate the first step, where only the effective thicknesses were fitted, and the second step where the effective thicknesses and optical properties of copper and copper oxide were fitted, respectively. The standard deviations of the effective thicknesses is given for the second step (between parentheses). They are lower than  $10^{-3}$  for the first step. **The uncertainty of  $t_C^b + t_O^b$  is calculated from uncertainties on  $t_C^b$  and  $t_O^b$  by using the square root of the sum of square [29].**

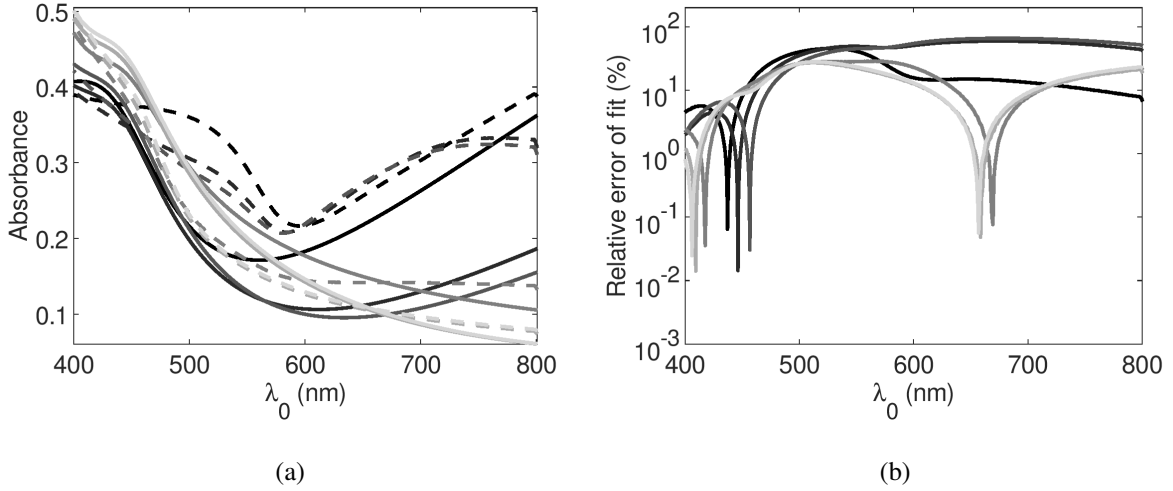


Figure 4: (a) Experimental absorbances (dashed lines) and best fits (solid lines) for the 6 samples  $t_C^a = 10$  nm. The color of plots is lighter for further oxidation steps. (b) Relative error of fit (Eq. 3).

133 From recommendations in Ref. [29], we have selected the best solutions with a tolerance of  
 134 10% (i.e. those with values of the fitness function smaller than the best one time 1.1). The se-  
 135 lected elements that satisfy this tolerance are a family of good solutions that helps to evaluate  
 136 uncertainties on the recovered data.

137 The plots of the experimental absorbance and of their best fit are shown in Fig. 4-6. **The posi-  
 138 tion of the minima of absorbance differs in experimental and fitted curves. Furthermore, the fitted  
 139 values of the thicknesses do not match with the AFM values. This confirms that the permittivities  
 140 of bulk materials are not suitable for the thin layers.** Therefore, we propose a second step, for  
 141 which both the effective thicknesses and the effective relative permittivities are taken as variables  
 142 of the fitting function. We consider a possible variation of  $\pm 10\%$  for each parameter of the two  
 143 Drude-Lorentz law of dispersion.

### 144 3.2. Second step: recovering of effective thicknesses and optical properties by perturbation

145 We use the effective thicknesses obtained in the previous subsection ( $t_C^a$  and  $t_O^a$  in Tab. 4) as  
 146 starting point and we consider an interval of search defined as  $t_C^b \in [\max(\{t_C^a - 10; 0\}); t_C^a + 10]$  nm.  
 147 Moreover, the boundaries of the interval of search for the fit of the relative permittivities are  
 148 calculated from the values in Tab. 3  $\pm 10\%$ . The size of the space of search is increased by  $\pm 20\%$

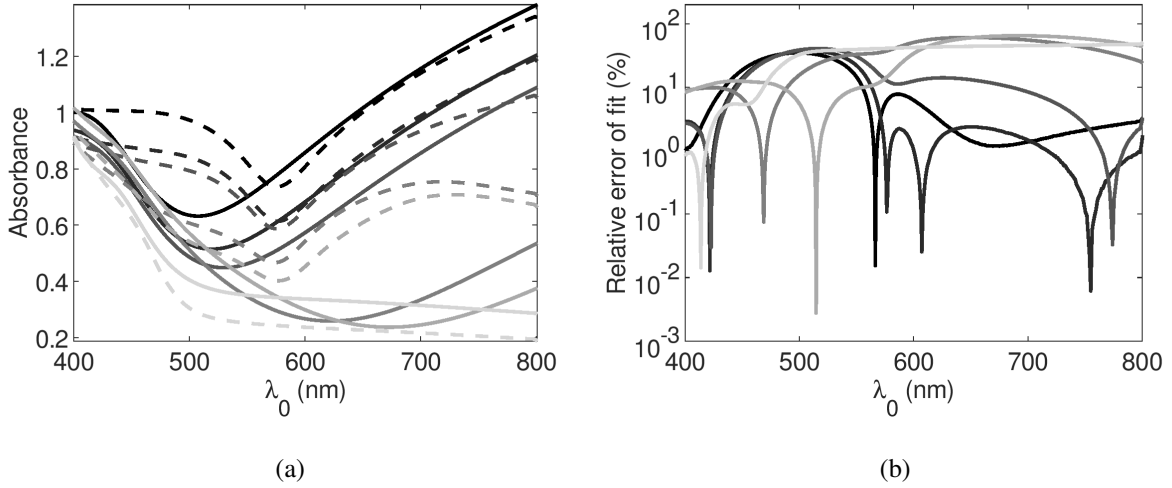


Figure 5: (a) Experimental absorbances (dashed lines) and best fits (solid lines) for the 6 samples  $t_C^n = 30$  nm. The color of plots is lighter for further oxidation steps. (b) Relative error of fit (Eq. 3).

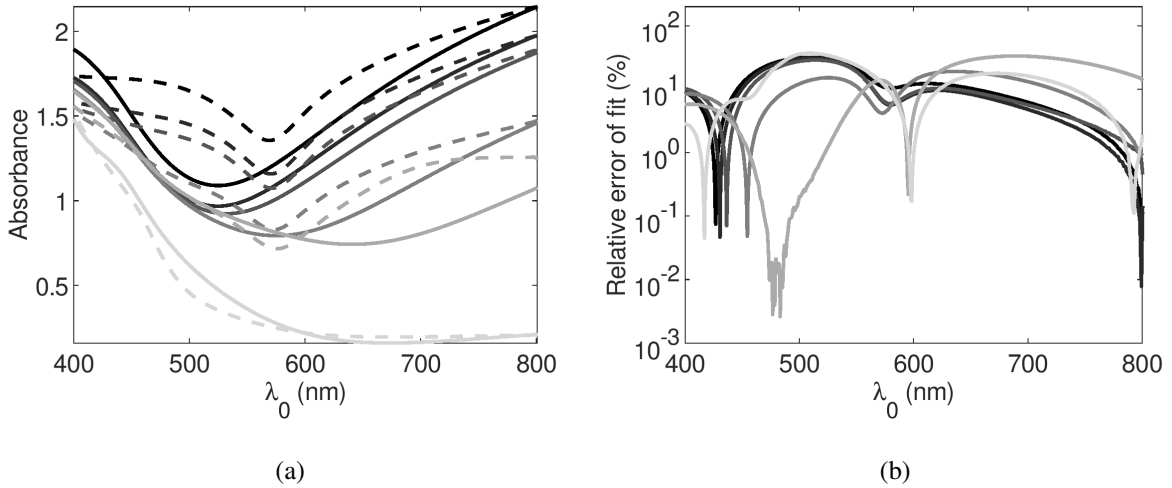


Figure 6: (a) Experimental absorbances (dashed lines) and best fits (solid lines) for the 6 samples  $t_C^n = 50$  nm. The color of plots is lighter for further oxidation steps. (b) Relative error of fit (Eq. 3).

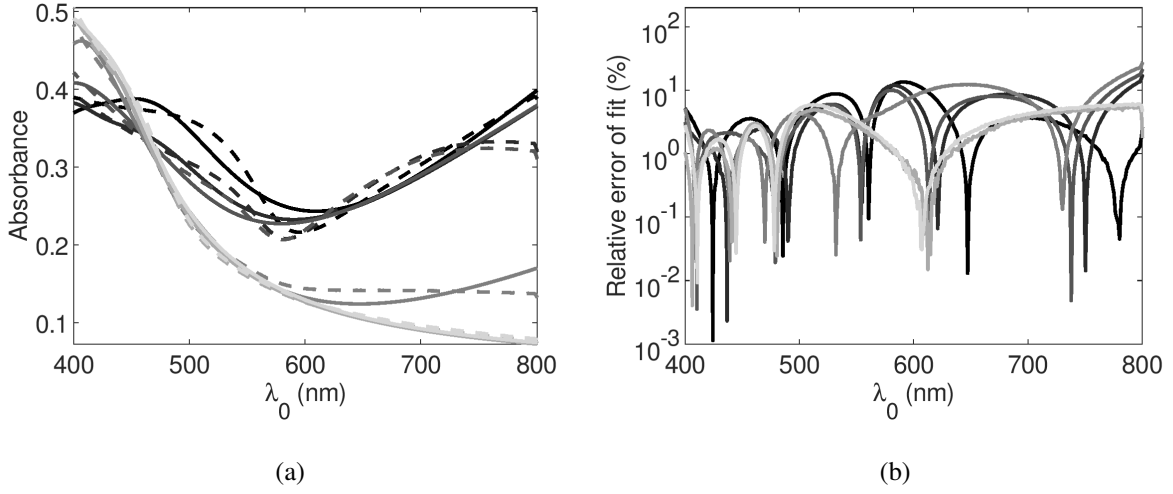


Figure 7: (a) fit of absorbance (solid line) and experimental absorbance (dashed line) for the 6 samples  $t_C^n = 10$  nm. The color of plots is becoming lighter for further oxidation steps. (b) relative fit error of fit (Eq. 3).

149 if the method fails to give a value of the fitness function smaller than 0.1. The values of the fitness  
 150 function  $E_f^b$  and thicknesses  $t^b$  are given in Tab. 4. Typically, the uncertainties on the recovered  
 151 effective thicknesses is lower than  $\pm 2$  nm, excepted for the sample (50, 600) for which the value of  
 152 the objective function is 0.1. In this case, the space of search for the optical properties is probably  
 153 still too tight.

154 The experimental absorbances and the fits are shown in Figs. 7-9. The color of the curves  
 155 varies from black to gray as a function of the oxidation time  $T$ . Therefore, the color of curves is  
 156 increasingly lighter when the residual effective thickness of copper decreases. Figures 10-11 show  
 157 the recovered effective relative permittivities for all investigated samples.

### 158 3.3. Discussion

159 For each of the 18 samples, a comparison of the values of the fitness function  $E_f^a$  and  $E_f^b$   
 160 is shown in Tab. 4. The initial effective thicknesses of copper ( $T = 0$  min), for each sample  
 161 ( $t_C^n = 10, 30, 50$  nm), is closer to the AFM values (Tab. 1) than in the first step, and taking into  
 162 account the uncertainties, practically match for all samples (less than 2% discrepancy for 10 nm  
 163 sample, and within the uncertainties intervals for the 30 nm and 50 nm samples). This further  
 164 confirms that the permittivities of thin layers differ from those of bulk materials. For each sample,

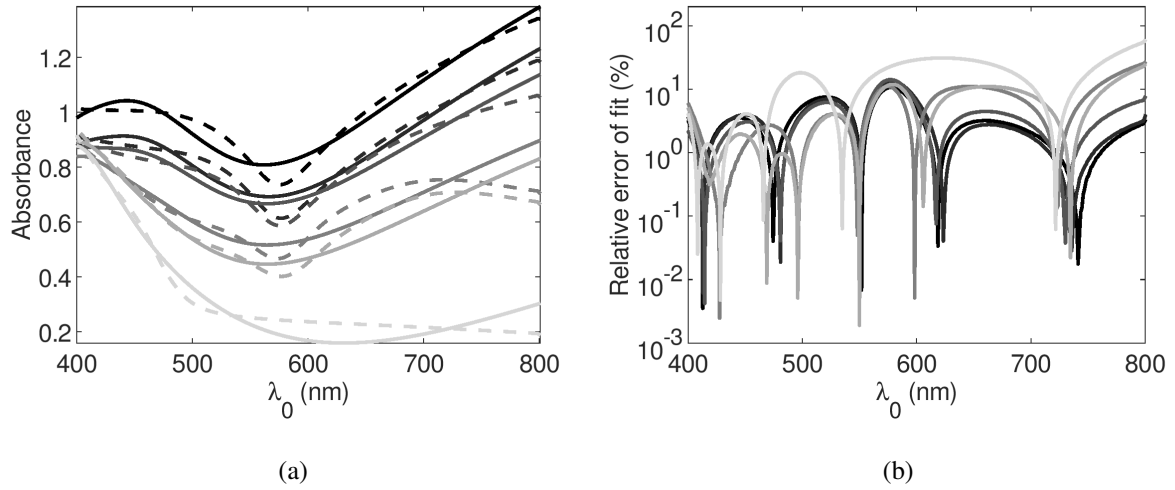


Figure 8: (a) fit of absorbance (solid line) and experimental absorbance (dashed line) for the 6 samples  $t_C^n = 30$  nm. The color of plots is becoming lighter for further oxidation steps. (b) relative fit error of fit (Eq. 3).

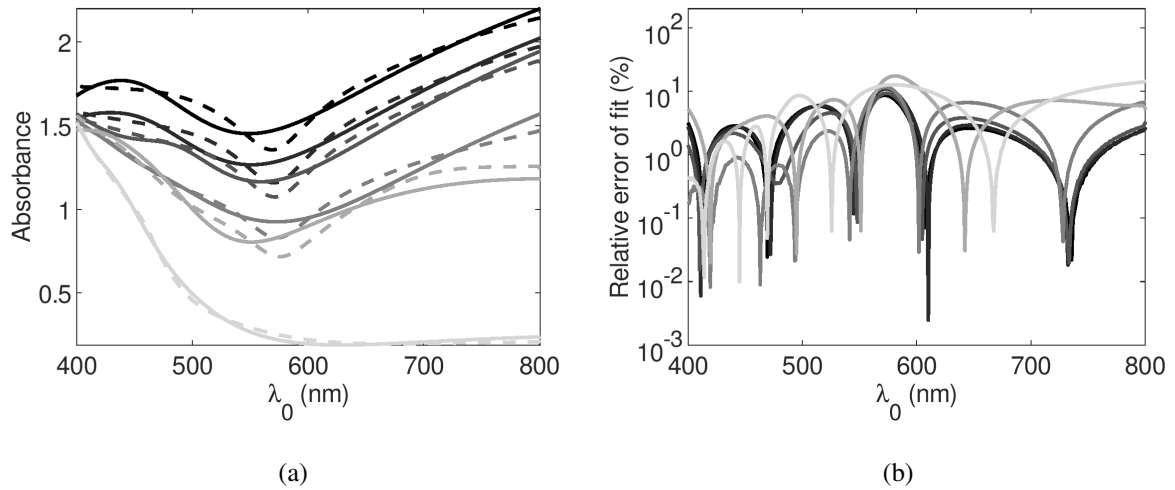


Figure 9: (a) fit of absorbance **data** (solid lines) and experimental absorbance (dashed lines) for the 6 samples  $t_C^m = 50$  nm. The color of plots is becoming lighter for further oxidation steps. (b) relative error of fit (Eq. 3).

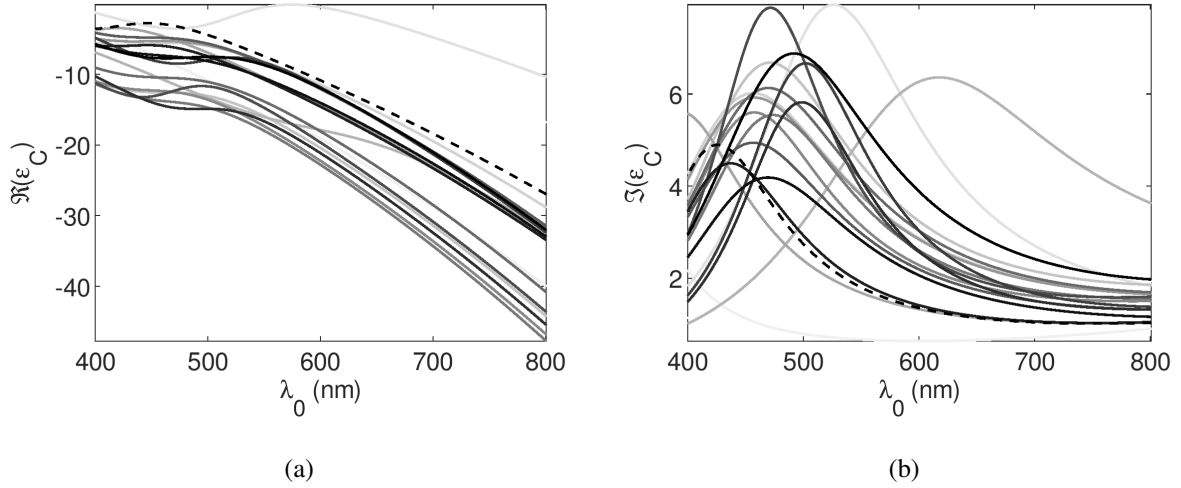


Figure 10: (a) Real part and (b) imaginary part of the recoveredfitted relative permittivity of copper. Dashed line: relative permittivity of the bulk materials. The color of plots is lighter for further oxidation steps.

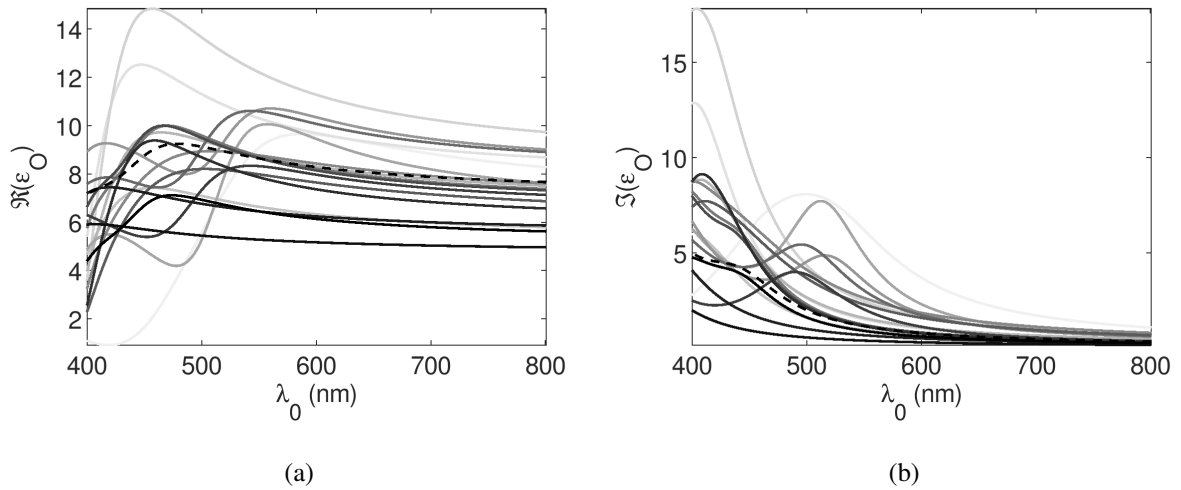


Figure 11: (a) Real part and (b) imaginary part of the recovered relative permittivity of copper oxide. Dashed line: relative permittivity of the bulk materials. The color of plots is darker for further oxidation steps.

165 the effective thickness of copper  $t_C^b$  is globally decreasing with oxidation time, and that of oxide  $t_O^b$   
166 is increasing. From a metrological point of view, the uncertainties must be enlarged to calculate  
167 confidence intervals. The confidence intervals are deduced from the uncertainties by enlarging by  
168 a coefficient  $k = 2$  in order to define a confidence level of 95% if the distribution of data follows a  
169 gaussian law [29] (the confidence level would be only 67% with  $k = 1$ , therefore considering only  
170 the standard deviation). The confidence intervals of the thickness of copper/copper oxide ( $t_C + t_O$ )  
171 measured by AFM, ellipsometry and fit of absorbance can be compared. The confidence inter-  
172 vals for AFM measurements are respectively [5.0; 17.0] nm, [21.0; 41.0] nm and [35.0; 67.0] nm  
173 for the three samples. They are wider than those for ellipsometry and fit of absorbance mea-  
174 surements due to the roughness of the sample. The corresponding values for fit of absorbance  
175 (step 1, 18 nm, 44 nm, 81 nm) are greater than the upper boundary of the confidence intervals.  
176 The confidence intervals of ellipsometry measurements is close to the upper boundary especially  
177 for the 30 nm target thickness ([13.8; 15.0] nm, [39.8; 45.0] nm). This behavior is coherent with  
178 the results of step 1: the effective measured thicknesses of copper are larger than the real one,  
179 due to both the roughness and the use of bulk permittivity. This global effect is confirmed by  
180 the ellipsometry and fit of absorbance measurements (step 1) of effective thicknesses of copper  
181 ([10.6; 11.4] nm, [36.1; 41.3] nm vs 12 nm, 38 nm (and 63 nm)). On the other hand, the effective  
182 thicknesses of copper oxide differs greatly for ellipsometry and fit of absorbance: [3.0; 3.8] nm vs  
183 6 nm, [3.3; 4.1] nm vs 6 nm, and [3.2; 6.8] nm vs 18 nm. This result reveals the high sensitivity of  
184 the effective thicknesses of thin oxide layer, to the models of dispersion (Eq. 4). However, from  
185 fit of absorbance (step 2), the recovered effective thicknesses are coherent with AFM measure-  
186 ments:  $t_C^b + t_O^b \in [13.7; 16.9]$  nm vs [5.0; 17.0] nm,  $t_C^b + t_O^b \in [34.4; 41.2]$  nm vs [21.0; 41.0] nm and  
187  $t_C^b + t_O^b \in [53.5; 61.9]$  nm vs [35.0; 67.0] nm. Note that the same conclusion could be drawn for  
188 confidence intervals at 67% ( $k = 1$ ). The thicknesses of copper are offset downward for fit of ab-  
189 sorbance (step 2), with reference to ellipsometry results. This reveals that the effective absorbance  
190 of nanometric layers of copper is higher than that of bulk (Fig.11 (b)). The effective thicknesses of  
191 very thin layers of oxide for fit of absorbance (step 2) are close to the ellipsometry ones excepted  
192 for the sample with 30 nm target thickness, despite a high variation of recovered effective optical  
193 properties (Fig. 11). This effect is due to the loss of sensitivity of the model to the oxide layer, the

194 absorbance being mainly dependent of the thicker copper layer. This explains why the effective  
195 thicknesses appear coherent between ellipsometry and fit of absorbance measurements, even if  
196 their optical properties differ.

197 Figures 7-9 exhibit a better position of the minimum and shape of the fit than in Figs. 4-  
198 6, which supports again that the fitted permittivities lead to a better description of the optical  
199 properties than those of bulk materials. Figures 10-11 show a global behavior of the recovered  
200 effective relative permittivities: when the effective thickness of materials decreases, the recovered  
201 effective relative permittivities get away from the bulk values. However, copper presents a shift of  
202 the maximum in the imaginary part of its effective relative permittivity. Its real (resp. imaginary)  
203 part appears smaller (resp. larger) than that of the bulk as expected, excepted for the smaller  
204 effective thicknesses. Therefore, the resolution of the inverse problem for the very thin layers of  
205 copper and oxide gives a set of parameters for the effective refractive index, that are far from the  
206 bulk values. Nevertheless, the structure of the materials in this case could make the model of plane  
207 layer questionable. The shape of the recovered real and imaginary parts also differ from that of the  
208 bulk. A global blue shift of the maximum of the imaginary part can be observed. A red shift of  
209 the maxima of both real and imaginary parts for larger effective thicknesses relatively to the bulk  
210 seems to be systematic for both materials. Even if the seven parameters of each Drude-Lorentz  
211 laws can vary from the bulk values by  $\pm 10\% - 20\%$ , inducing a possible variation of the relative  
212 permittivity of more than 70% over the spectrum, the best fit remains close to the bulk dispersion  
213 curve.

#### 214 4. Conclusion

215 The main result of this paper is a first evidence of the possibility of using absorbance spectra for  
216 recovering both the effective thicknesses and relative permittivities of a metal-oxide bilayer. The  
217 application of the method to 18 samples shows that the results are coherent, and in fair agreement  
218 with AFM measurements as revealed by the overlap of the confidence intervals. Results calculated  
219 in step 1 of our method, assuming the optical properties of bulk materials as in ellipsometry, show  
220 a similar global behavior: the effective thicknesses are greater than those measured by AFM, on  
221 the contrary to the thicknesses obtained from step 2. The relative uncertainties of the thicknesses

222 obtained from the fit of absorbance spectra (step 2) and from ellipsometry are of the same order of  
223 magnitude. Moreover, the effective relative permittivities recovered significantly differ from the  
224 bulk ones for nanometric thicknesses. Of course, the recovered thicknesses and optical properties  
225 are effective values as in ellipsometry, assuming the flatness and the homogeneity of the bilayer.  
226 The preliminary knowledge of material structure (porosity, crystallinity. . . ) could help to improve  
227 the choice of the model of interaction between light and matter. However, the method may be used  
228 to characterize a multilayer and the recovered parameters, depending on the process of deposition  
229 and annealing of the layers, which could be used to optimize setups.

## 230 Acknowledgement

231 Deniz Cakir, Nicole Fréty and Eric Anglaret thank Atotech GmbH for financial support as well  
232 as Senguel Karasahin and Matthias Dammasch for their help in the ellipsometry measurements.  
233 They also thank Michel Ramonda from the Université de Montpellier for his precious help in the  
234 AFM measurements.

## 235 References

- 236 [1] I. Y. Erdogan, O. Gullu, Optical and structural properties of cuo nanofilm: Its diode application, *J. Alloy. Compd.*  
237 492 (2010) 378–383.
- 238 [2] J. Watanabe, A. Takeuchi, Y. Uehara, S. Ushioda, Prism-coupled light emission from tunnel junctions containing  
239 interface roughness experiment, *Phys. Rev. B* 38 (18) (1988) 12959–12965.
- 240 [3] S. Kessentini, D. Barchiesi, Nanostructured Biosensors Influence of Adhesion Layer, Roughness and Size on  
241 the LSPR A Parametric Study, INTECH Open Access, 2013, Ch. 12, pp. 311–330, iSBN 978-953-51-1004-0.
- 242 [4] D. L. Mills, Attenuation of surface polaritons by surface roughness, *Phys. Rev. B* 12 (10) (1975) 4036–4046,  
243 (Erratum in *Phys. Rev. B* 14, 5539 (1976)).
- 244 [5] S. A. Meyer, B. Auguié, E. C. L. Ru, P. G. Etchegoin, Combined SPR and SERS microscopy in the Kretschmann  
245 configuration, *J. Phys. Chem. A* 116 (2012) 1000–1007.
- 246 [6] D. Barchiesi, T. Grosge, F. Colas, M. Lamy de la Chapelle, Combined SPR and SERS Otto and Kretschmann  
247 configurations, *J. Opt.* 17 (11) (2015) 114009 (10 pp.).
- 248 [7] R. Gillibert, M. N. Triba, M. L. de la Chapelle, Surface enhanced raman scattering sensor for highly sensitive  
249 and selective detection of ochratoxin a, *The Analyst* 1 (2017) 143.

- 250 [8] J. M. Bennet, Measurement of the rms roughness, autocovariance function and other statistical properties of  
251 optical surfaces using FEKO scanning interferometer, *Appl. Opt.* 15 (11) (1976) 2705–2721.
- 252 [9] K. M. Byun, S. J. Yoon, D. Kim, Effect of surface roughness on the extinction-based localized surface plasmon  
253 resonance biosensor, *Appl. Opt.* 47 (1) (2008) 5886–5892.
- 254 [10] K. M. Byun, S. J. Yoon, D. Kim, S. J. Kim, Sensitivity analysis of a nanowire-based surface plasmon resonance  
255 biosensor in the presence of surface roughness, *J. Opt. Soc. Am. A* 24 (2) (2007) 522–529.
- 256 [11] S. Kessentini, D. Barchiesi, Roughness effect on the efficiency of dimer antenna based biosensor, *Advanced  
257 Electromagnetics* 1 (2) (2012) 41–47.
- 258 [12] A. Trügler, J.-C. Tinguely, J. R. Krenn, A. Hohenau, U. Hohenester, Influence of surface roughness on the optical  
259 properties of plasmonic nanoparticles, *Phys. Rev. B* 83 (2011) 081412–1–081412–4.
- 260 [13] L. G. Shultz, The optical constants of silver, gold, copper and aluminum. I. the absorption coefficient  $k$ , *J. Opt.  
261 Soc. Am.* 44 (5) (1954) 357–362.
- 262 [14] L. G. Shultz, F. R. Tangherlini, The optical constants of silver, gold, copper and aluminum. II. the index of  
263 refraction  $n$ , *J. Opt. Soc. Am.* 44 (5) (1954) 362–368.
- 264 [15] A. Bruckbauer, A. Otto, Raman spectroscopy of pyridine adsorbed on single crystal copper electrodes, *J. Raman  
265 Spectrosc.* 29 (8) (1998) 665–672.
- 266 [16] M. Shanidand, M. Abdul Khadar, V. G. Sathe, Fröhlich interaction and associated resonance enhancement in  
267 nanostructured copper oxide films, *J. Raman Spectrosc.* 42 (9) (2011) 1769–1773.
- 268 [17] K. Fujita, D. Ando, M. Uchikoshi, K. Mimura, M. Isshiki, New model for low-temperature oxydation of copper  
269 single crystal, *Appl. Surf. Sci.* 276 (2013) 347–358.
- 270 [18] V. Figueiredo, E. Elangovan, G. Goncalves, P. Barquinha, L. Pereira, N. Franco, E. Alves, R. Martins, E. For-  
271 tunato, Effect of post-annealing on the properties of copper oxide thin films obtained from the oxidation of  
272 evaporated metallic copper, *Appl. Surf. Sci.* 254 (13) (2008) 3949–3954.
- 273 [19] K. M. McPeak, S. V. Jayanti, S. J. P. Kress, S. Meyer, S. Iotti, A. Rossinelli, D. J. Norris, Plasmonic films can  
274 easily be better rules and recipes, *ACS Photonics* 2 (3) (2015) 326–333.
- 275 [20] M. O’Reilly, X. Jiang, J. T. Beechinor, S. Lynch, C. NiDheasuna, J. C. Patterson, G. Crean, Investigation of the  
276 oxidation behaviour of thin film and bulk copper, *Appl. Surf. Sci.* 91 (1995) 152–156.
- 277 [21] M. Ramirez, L. Henneken, S. Virtanen, Oxidation kinetics of thin copper films and wetting behaviour of copper  
278 and organic solderability preservatives (OSP) with lead-free solder, *Appl. Surf. Sci.* 257 (15) (2011) 6481–6488.
- 279 [22] A. Yabuki, S. Tanaka, Oxidation behavior of copper nanoparticles at low temperature, *Mater. Res. Bull.* 46 (12)  
280 (2011) 2323–2327.
- 281 [23] N. A. Raship, M. Z. Sahdan, F. Adriyanto, M. F. Nurfazliana, A. S. Bakri, Effect of annealing temperature on  
282 the properties of copper oxide films prepared by dip coating technique, in: *AIP Conf. Proc.*, Vol. 1788, 2017, p.  
283 030121.

- 284 [24] Y. Zhu, K. Mimura, J.-W. Lim, M. Isshiki, Q. Jiang, Brief review of oxidation kinetics of copper at 350°C to  
285 1050°C, *Metall. Mater. Trans. A* 37A (2006) 1231–1237.
- 286 [25] C. Gattinoni, A. Michaelides, Atomistic details of oxide surfaces and surface oxidation: the example of copper  
287 and its oxides, *Surf. Sci. Rep.* 70 (2015) 424–447.
- 288 [26] S. Choudhary, J. V. N. Sarma, S. Gangopadhyay, Growth and characterization of single phase Cu<sub>2</sub>O by thermal  
289 oxidation of thin copper films, in: *AIP Conf. Proc.*, Vol. 1724, 2016, p. 020116.
- 290 [27] D. Barchiesi, A 3-D multilayer model of scattering by nanostructures. application to the optimisation of thin  
291 coated Nano-Sources, *Opt. Commun.* 126 (1996) 7–13.
- 292 [28] D. Barchiesi, T. Grosjes, Fitting the optical constants of gold, silver, chromium, titanium, and alu-  
293 minium in the visible bandwidth, *J. Nanophoton.* 8 (1) (2014) 089996 (083097), erratum 2015 089996. doi  
294 10.1117/1.JNP.8.089996.
- 295 [29] D. Barchiesi, T. Grosjes, Propagation of uncertainties and applications in numerical modeling: tutorial, *J. Opt.*  
296 *Soc. Am. A* 34 (9) (2017) 1602–1619.
- 297 [30] SOPRA (2018). URL <http://www.sspectra.com/sopra.html>
- 298 [31] W. Gao, H. Hong, J. He, A. Thomas, L. Chan, S. Li, Oxidation behaviour of Cu thin films on Si wafer at 175-400  
299 °C, *Materials Letters* 51 (2001) 78–84.
- 300 [32] J. Iijima, J. W. Lim, Hong, S. H., S. Suzuki, M. Mimura, K. and Isshiki, Native oxidation of ultra high purity Cu  
301 bulk and thin films, *Appl. Surf. Sci.* 253 (5) (2006) 2825–2829.
- 302 [33] D. Barchiesi, Improved method based on S matrix for the optimization of SPR biosensors, *Opt. Commun.* 286 (1)  
303 (2013) 23–29.
- 304 [34] G. Ghosh, Dispersion-equation coefficients for the refractive index and birefringence of calcite and quartz crys-  
305 tals, *Opt. Commun.* 163 (1999) 95–102.
- 306 [35] D. Barchiesi, Numerical retrieval of thin aluminium layer properties from SPR experimental data, *Opt. Express*  
307 20 (8) (2012) 9064–9078.
- 308 [36] D. Barchiesi, The Lycurgus cup inverse problem using photographs for characterization of matter, *J. Opt. Soc.*  
309 *Am. A* 32 (8) (2015) 1544–1555.
- 310 [37] D. Macías, A. Vial, D. Barchiesi, Evolution strategies approach for the solution of an inverse problem in near-  
311 field optics, in: G. Raidl, S. Cagnoni, J. Branke, R. Corne, D.W. and Drechsler, Y. Jin, C. Johnson, P. Machado,  
312 E. Marchiori, F. Rothlauf, G. Smith, G. Squillero (Eds.), *Lecture Notes in Computer Science* (6e European  
313 Workshop on Evolutionary Computation in Image Analysis and Signal Processing), Vol. 3005 / 2004, Springer-  
314 Verlag Heidelberg, Germany, 2004, pp. 329–338.
- 315 [38] D. Macías, D. Barchiesi, Identification of unknown experimental parameters from noisy apertureless scanning  
316 near-field optical microscope data with an evolutionary procedure, *Opt. Lett.* 30 (19) (2005) 2557–2559.
- 317 [39] D. Macías, A. Luna, D. Skigin, M. Inchaussandague, A. Vial, D. Schinca, Retrieval of relevant parameters of

- 318 natural multilayer systems by means of bio-inspired optimization strategies, *Appl. Opt.* 52 (11) (2013) 2511–  
319 2520.
- 320 [40] Y. Shi, R. C. Eberhart, A modified particle swarm optimizer, in: *Proc. IEEE Congress on Evolutionary Compu-*  
321 *tation (CEC'98)*, Anchorage, AK, 1998, pp. 69–73.